Original Article

MOLECULAR METABOLISM

The disassembly of the neuromuscular synapse in high-fat diet-induced obese male mice

Isabel Martinez-Pena y Valenzuela [1], Mohammed Akaaboune [1,2,*]

ABSTRACT

Objective: A sustained high fat diet in mice mimics many features of human obesity. We used male and female Non-Swiss albino mice to investigate the impact of short and long-term high-fat diet-(HFD)-induced obesity on the peripheral neuromuscular junction (NMJ) and whether obesity-related synaptic structural alterations were reversible after switching obese mice from HFD to a standard fat diet (SD).
Methods: HFD-induced obese and age-matched control mice fed SD were used. We carried out in vivo time lapse imaging to monitor changes of synapses over time, quantitative fluorescence imaging to study the regulation of acetylcholine receptor number and density at neuromuscular junctions, and high resolution confocal microscope to study structural alterations in both the pre- and postsynaptic apparatus.
Results: Time-lapse imaging in vivo over a 9 month period revealed that NMJs of HFD obese male mice display a variety of obesity-related structural alterations, including the disappearance of large synaptic areas, significant reduction in the density/number of nicotinic acetylcholine receptor (AChRs), abnormal distribution of AChRs, high turnover rate of AChRs, retraction of axons from lost postsynaptic sites, and partially denervated synapses. The severity of these synaptic alterations is associated with the duration of obesity. However, no substantial alterations were observed at NMJs of age-matched HFD obese female mice or male mice fed with a standard or low fat diet. Intriguingly, when obese male mice were switched from HFD to a standard diet, receptor density and the abnormal pattern of AChR distribution were completely reversed to normal, whereas lost synaptic structures were not restored.
Conclusions: These results show that the obese male mice are more vulnerable than female mice to the impacts of long-term HFD on the NMJ damage and provide evidence that diet restriction can partially reverse obesity-related synaptic changes.

Keywords High-fat diet induced obesity; Neuromuscular junction alterations; In vivo imaging; Neurotransmitter acetylcholine receptors; Metabolic stability of AChRs; Muscle denervation; Standard diet

1. INTRODUCTION

Obesity, a serious human disease, is associated with several chronic conditions including hypertension, type-2 diabetes and cancer [1]. Obesity is characterized by an excessive accumulation of adipose tissue and a significant increase of body mass index [2,3]. Monogenic animal models of obesity, such as ob/ob mice (in which leptin, the fat-derived hormone that is involved in food intake and body weight, is deficient), leptin receptor deficient db/db mice, and MC4 receptor deficient mice, have been useful in studying the role of individual genes in the formation of fat cells and understanding signaling pathways involved in obesity [4–9]. Diet-induced-obesity mouse models [10–12], which mimic many aspects of human obesity, have also been useful for investigating the relationship between high-fat Western diets and the development of obesity as well as the mechanisms by which dietary composition contributes to the regulation of body weight.
Obesity-related metabolic syndromes have been extensively studied for decades [13]. However, the effects of obesity on the nervous system, particularly on the structure and function of the peripheral nervous system, have been largely overlooked. In obese mice, it has been reported that obesity is associated with a decline in cognitive performance [14,15], a decrease in the formation of new dendritic spines, and dysfunction of neuronal plasticity [16,17]. For instance, in the hypothalamic brain area of obese mice deficient in leptin, leptin receptor, or in high fat diet (HFD) obese mouse models, the number and function of excitatory and inhibitory synaptic inputs to the neuropeptide Y, proopiomelanocortin, and to orexin-A neurons were altered [18]. Similarly, in the hippocampus of obese mice, synaptic alterations in neuronal circuitries were observed [19], suggesting that obesity may affect learning and memory. Likewise, in patients with obesity, there is evidence for decreased hippocampal size and cognitive impairments [20]. At present, the short and long term effects of obesity induced by HFD on the maintenance of the neuromuscular junction (NMJ) remain largely unknown.
In this study, we investigated whether obesity itself in the absence of other obvious associated conditions has any consequences on the stability of the NMJ over time. For this, we used Non-Swiss albino male and female mice, and a non-diabetic and non-hyperglycemic mouse model of diet-induced obesity. We found that obese male mice were more vulnerable than obese females to the impacts of HFD on the

[1]Department of Molecular, Cellular, and Developmental Biology, USA [2]Program in Neuroscience, University of Michigan, Ann Arbor, MI, 48109, USA

*Corresponding author. Mohammed Akaaboune, PhD Dept of Molecular, Cellular and Developmental Biology Neuroscience program 4160 Biological Sciences Building 1105 N. University Avenue University of Michigan, Ann Arbor, USA Fax: +734 647 0884. E-mail: makaabou@umich.edu (M. Akaaboune).

Received January 27, 2020 • Revision received March 9, 2020 • Accepted March 10, 2020 • Available online 18 March 2020

https://doi.org/10.1016/j.molmet.2020.100979

structural integrity of the NMJ and the metabolic stability of AChR. Particularly, we found that HFD obese male mice displayed multiple alterations in the structure of the NMJ and in the number and distribution of AChRs, only some of which were reversible upon switching to a standard diet.

2. MATERIALS AND METHODS

2.1. Animals and diets

All animal protocols were approved by the Institutional Animal Care & Use Committee of the University of Michigan.

Non-Swiss Albino mice were fed regular chow (Standard diet, SD), low fat diet (LFD) or HFD (HFD) *ad libitum*. SD was obtained from PicoLab Laboratory Rodent Diet. In this diet, 28.67% of the total calories are provided by proteins, 13.38% of calories originate from fat, and 57.94% of calories from carbohydrates. HFD (D12492, Research Diets, Inc) composition has 60% of the total calories provided by fat (lard), while 20% are supplied by proteins and the remaining 20% comes from carbohydrates. LFD (D12450B, Research Diets, Inc.) contains the same ingredients with a closely matched composition to the HFD: Twenty percent of the total calories are provided by proteins, 10% of calories originate from fat, and 70% of calories from carbohydrates. After weaning at 21 days old, mice were weighed weekly and maintained on the above diets for up to 9 months of age. The mice had unlimited access to food and water.

2.2. Metabolism characterization

Monitoring blood glucose: Blood glucose concentration was measured with a blood glucose monitoring system based on an amperometric electrochemistry assay (Accu-Chek Performa Strips and Glucometer, Roche Diagnostics, Australia). Blood samples were collected from the tail vein at $\sim$2 week intervals and placed into blood glucose test strips with an assay range of 20–500 mg/dl. The data were expressed as standard deviation of mean (mean $\pm$ SD).

Glucose Tolerance Tests: To measure blood glucose levels, blood samples were taken from the tail of overnight fasted mice before (t = 0 min) and at subsequent time intervals following intraperitoneal administration of 2 g glucose/kg body mass. Blood glucose levels were measured using Accu-Chek Performa Strips and Glucometer (Roche Diagnostics, Australia).

Insulin tolerance test: Intraperitoneal injection of insulin at a concentration of 0.75 IU/g body mass was administered to mice fasted for six hours and blood glucose levels were measured using Accu-Chek Performa Strips and Glucometer over a 2-hour interval.

2.3. In vivo imaging, quantitative fluorescence assay, and confocal microscopy

For in vivo experiments, each mouse was studied at two time points (2 and 4 months, 4 and 6 months, 7 and 9 months, or 5 and 9 months). Prior to imaging, mice were anesthetized with intraperitoneal injections of a mixture of 80 mg/kg ketamine and 20 mg/kg xylazine. The sternomastoid muscle was exposed, bathed with BTX-Alexa488 (5 μg/ml, 5 min) and superficial NMJs were imaged and then re-imaged 2–4 months later using a standard epifluorescence microscope as described previously [21,22].

To determine the density of postsynaptic AChRs, muscles were bathed with a saturating dose of BTX-Alexa488 (5 μg/ml, 1 h) and superficial receptors at NMJs were imaged. To determine the turnover rate of AChR, muscles were bathed with a low dose of BTX-Alexa488 (5 μg/ml, 5 min) and superficial NMJs were imaged and re-imaged 3 or 7 days later. The fluorescence intensity of labeled receptors was assayed using a procedure written for Matlab (The Mathworks). Briefly, the background fluorescence was approximated by selecting a boundary region around the NMJ and subtracting it from the original image, and the mean of the total fluorescence intensity (which corresponds to density) was measured [21,23,24].

In another series of experiments, muscles (sternomastoid, soleus, and EDL) were fixed in 4% PFA and bathed with BTX-Alexa488 (to label AChRs) and fasciculin2 Alexa-594 (to label AChEs). The staining of nerve terminals was performed by incubating fixed sternomastoid muscles (9 month-old HFD and SD male mice) with neurofilament to visualize the axons (2H3, 1/100; Developmental Studies Hybridoma Bank). The NMJs were then imaged with a confocal microscope (Leica SP5) as described in our previous work [25]. The z-stacks were collapsed and the contrast adjusted with Adobe Photoshop.

To determine whether switching HFD obese male mice to SD has any impact on reversing postsynaptic alterations, mice fed with HFD at 6 months after initial feeding were switched from HFD to SD for 3 months. The body weight of mice was then measured and NMJs were imaged with a confocal microscope.

2.4. Fiber crossectional area

Cryosections were stained by Hematoxylin and Eosin, imaged using a Nikon E600 microscope and cross-sectional areas were analyzed with ImageJ software (NIH, version 1.49). We used the freehand toolbar to select areas of muscle section and the measure function to determine the area of the selected region after at least 50 muscle fibers per muscle, and four muscles per diet, were counted.

2.5. Statistics

All statistics were performed using GraphPad Prism software version 8.0.1. Significance was calculated by unpaired t-test with two-tailed P value. One-way Analysis of variance (ANOVA) was used to analyze statistical differences between more than two groups and a post hoc Tukey test for individual differences when appropriate. A P value < 0.05 was considered statistically significant.

3. RESULTS

3.1. Characterization of an HFD-induced obese mouse model

In this study, we used the Non-Swiss Albino mouse strain (CF1). Young male and female mice (21 days after birth) were divided randomly into three groups fed with different diets (see methods): The first group was fed an HFD; the second group was fed an SD; and the third group was fed an LFD. Weight gain as the primary effect of diet-induced obesity was measured from 21 days of age to up 9 months (Figure 1). The HFD male mice had gained significantly more weight than SD or LFD males over time (starting at $\sim$ 2 months) (Figure 1A), while there was no significant difference in body weight between females fed with HFD or SD during the first 5 months of HFD feeding (Figure 1B), consistent with previous studies [26,27]. However, from 6 to 9 months, the HFD female mice had gained more weight than SD fed females (Figure 1B). Next, we examined whether our HFD-induced obese mice were hyperglycemic and had developed diabetes. To do this, blood samples from male mice fed with HFD, SD, and LFD were collected at 8 weeks, 6 and 9 months and plasma glucose levels were measured. As shown in Figure 1C, there were no significant differences in blood glucose measurements between SD, LFD and HFD males. Similar results were obtained in females fed SD and HFD at either 6 months or 9 months (Figure 1D).

We also performed insulin tolerance (ITT) and glucose tolerance (GTT) tests to assess glucose metabolism in 9-month-old HFD male mice.

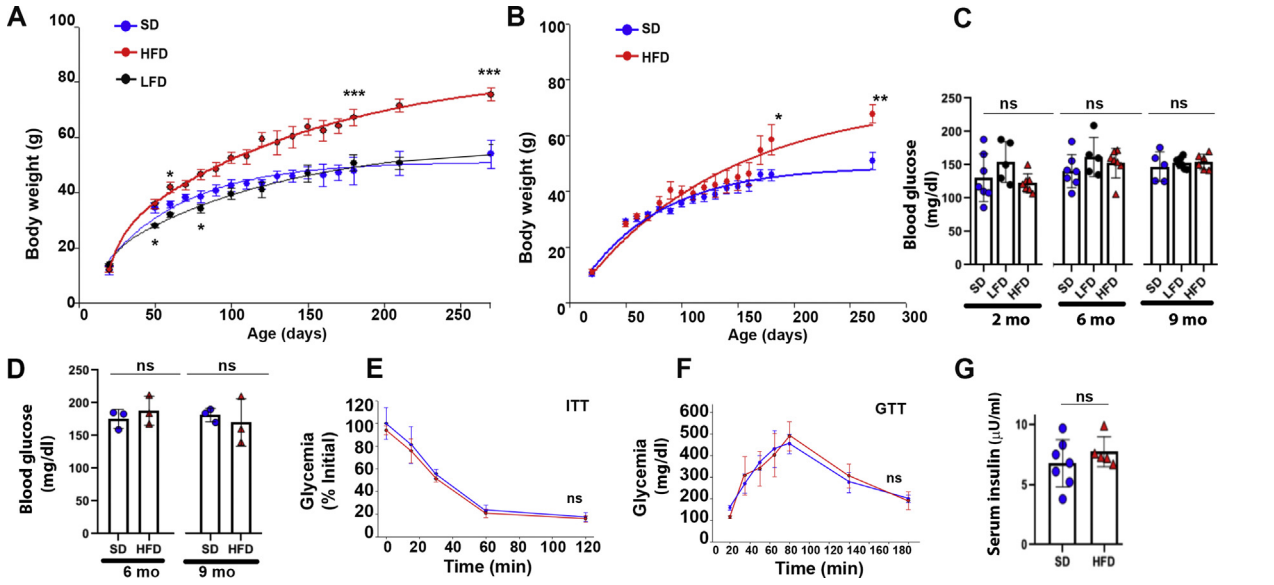

Figure 1: Metabolic characterization of Non-Swiss Albino mice. A. Body weight of standard diet (SD) (n = 15), low fat diet (LFD) (n = 10) and high fat diet (HFD) (n = 20) fed male mice up to 270 days of age. Data are means ± SEM. *p < 0.01 and ***p < 0.0001 vs SD. **B**. Body weight of SD (n = 10) and HFD (n = 10) fed female mice up to 270 days of age. Data are means ± SEM. *p < 0.01 and **p < 0.001 vs SD. **C**. Non-fasting blood glucose concentrations from males at 2 [HFD-fed mice was 123 ± 12 mg/dl (n = 7), SD-fed mice was 130 ± 35 (n = 7) and the LFD group was 154 ± 30 mg/dl (n = 5), p = 0.33], 6 [HFD group was 153 ± 27 mg/dl (n = 7), the SD group was 140 ± 16 (n = 7) and the LFD group was 162 ± 33 mg/dl (n = 5) p = 0.59], and 9 months (HFD 155 ± 12 (n = 6); SD 147 ± 7.6 (n = 5); LFD 152 ± 26 (n = 5); p = 0.7). Note that the values are similar between all three groups. Data are means ± SD. **D**. Non-fasting blood glucose concentrations from females at 6 [HFD: 188 ± 12 mg/dl (n = 3); SD: 176 ± 14 mg/dl (n = 3), p = 0.47], and 9 months [HFD: 170 ± 30 mg/dl (n = 3); SD 181 ± 10 mg/dl (n = 3); p = 0.63]. Data are means ± SD. **E**. Insulin Tolerance Test: IP injection of 0.75 IU/g (body weight) insulin in 9 months old HFD and SD male mice after 6 h fasting. IIT test shows no differences in blood glucose. Data are means ± SD. **F**. Glucose Tolerance Test. Blood glucose levels from overnight fasted SD and HFD male mice were measured at different time points after IP injection of 2 g of glucose/kg (body weight) showing no differences in blood glucose values. Data are means ± SD. **G**. Serum insulin concentrations from 9-month-old HFD and age-matched SD fed male mice showing no differences between both groups. Long term HFD induces body weight gain in male mice but are normoglycemic.

For the insulin tolerance test, six hour-fasted mice were injected intraperitoneally with insulin (0.75 IU/g body weight) and blood glucose levels were measured. As shown in Figure 1E, there was no significant change in blood glucose levels between HFD and SD mice at different time points (0, 15, 30, 60 and 120 min) after injection of insulin (p = 0.51, 3 mice per group). For the GTT, an intraperitoneal glucose dose (2 g/kg body weight) was administered to overnight fasted mice and blood glucose levels were measured at different time points after injection (Fig. 1F). The time to clear the glucose was similar between all groups (p = 0.7, 3 mice per group), suggesting that glucose tolerance was minimally disrupted by HFD. Similarly, there was no statistically significant difference in serum insulin concentration between 9-month-old HFD-fed mice and age-matched SD fed mice (Fig.1G). Altogether, these results strongly suggest that our obese male mice are non-diabetic and non-hyperglycemic.

3.2. Postsynaptic alterations of the neuromuscular system in high-fat-induced obese mice

To study the effects of obesity induced by HFD on the structural integrity of the NMJ, we used the power of time-lapse imaging to capture relevant changes (which can be easily overlooked in snapshot images). The sternomastoid muscles of aged matched obese and non-obese male and female mice that had been fed continuously with either HFD or SD were bathed with a low dose of BTX-Alexa488 (5 µg/ml, 5 min) that was used to label acetylcholine receptors (which mark synaptic sites) but was insufficient to prevent nerve evoked contractions [21]. Superficial synapses were then imaged immediately and re-imaged two months later with a fresh dose of BTX-Alexa488. In male mice, we found that over all three imaging windows (2—4 months, 4—6 months, and 7—9 months) there was a much greater loss of post-synaptic receptors at the second viewing in the HFD mice than in the SD mice (Table 1 and Figure 2A,B). One simple way to quantify the loss of AChR staining in HFD mice was to count the number of synaptic branches lost between two consecutive imaging sessions, where a synaptic branch was defined as a synaptic region that bifurcated from the main branch of the NMJ (Figure 2D). It is noteworthy to mention that the amount of synaptic branch loss we found in the non-Swiss albino mice on the SD was consistent with the normal process of synaptic remodeling at the adult NMJ previously reported for CF1 and C57BL/6 J mice [28—30], while the loss of synaptic branches in the HFD mice was much greater (Table 1). Table 1 also showed that the extent of the loss of synaptic branches in HFD obese male mice increased with the duration of obesity. Another way to quantify the extent of receptor loss was to measure the ratio of stained AChRs areas between the two viewings. As shown in Figure 2E, the ratio of stained

Table 1 — Lost Synaptic Branches in vivo.

Lost branches	2—4 months		4—6 months		7—9 months	
	SD	HFD *	SD	HFD †	SD	HFD †
0—1	16 (80%)	8 (24.2%)	14 (66.6%)	4 (13.8%)	13 (40.6%)	5 (17.2%)
2—5	4 (20%)	20 (60.6%)	7 (33.3%)	19 (65.5%)	17 (53.1%)	10 (34.5%)
>6	0	5 (15.1%)	0	6 (20.7%)	2 (6.2%)	14 (48.3%)
TOTAL NMJs	20	33	21	29	32	29

*Indicates significance compared to age-matched Standard Diet *(p<0.001)*,† Indicates significance compared to age-matched Standard Diet *(p<0.0001). 3—4 mice* per *diet* per *start age*.

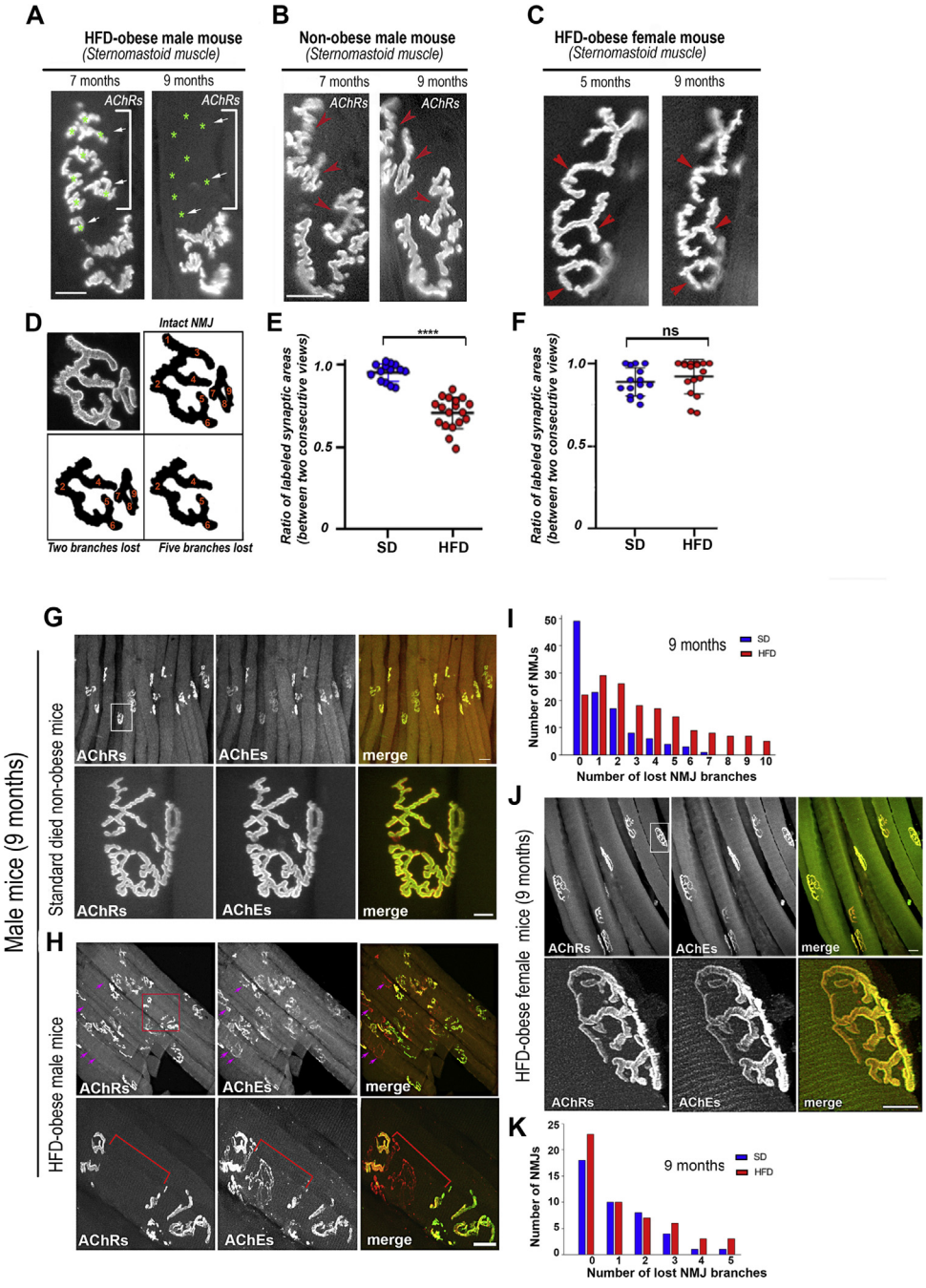

Figure 2: Time dependent changes in the structure of the NMJs of mice fed the HFD or the SD. The sternomastoid muscles of aged matched obese and non-obese male and female mice that had been fed continuously with either HFD or standard diet were bathed with a low dose of BTX-Alexa488 and superficial NMJs were imaged. **A.** The same synapse was imaged at 7 months and then again at 9 months in a male mouse fed the HFD from postnatal day 21 (green asterisks and arrows indicate the presence and absence of synaptic branches between the two views). **B.** The same synapse was imaged at 7 months and then again at 9 months in a male mouse fed the SD from postnatal day 21. **C.** The same synapse was imaged at 5 months and then again at 9 months in a female mouse fed the HFD from postnatal day 21. Red arrowheads in B and C indicate the presence of synaptic branches between the two views. **D.** Schematic to illustrate the method used to quantify the number of synaptic branches lost between two imaging sessions. **E** and **F**. Quantitative assessment of a series of images of male and female mice (as in A, B and C). The area of BTX fluorescence at each synapse was determined as described in methods, and then the ratio of the area of each synapse at 9 months relative to the area of the same synapse at 7 months (males) and at 5 months (females) was calculated (three mice for SD, four mice for HFD). (****$p < 0.0001$). **G-K.** Sternomastoid muscles of 9-month-old HFD obese and age-matched non-obese female and male mice were fixed and bathed with BTX-Alexa488 (green) to label AChRs, which mark postsynaptic sites and fasciculin2-Alexa594 (red) to label AChEs, which mark the original location of the synapses. NMJs were then imaged with a confocal microscope. **G** and **H**. Synapses from male mice on the standard diet (G) and a High Fat Diet (H). The top panels of G and H show a number of fibers, while the lower panels show the boxed region at higher power. **I**. Histograms showing number of branches lost from NMJs of SD and HFD at male 9-month-old. Note that there was a significant increase in the number of altered NMJs and loss of postsynaptic areas in HFD obese mice. **J**. Synapses from obese female mice on the High Fat Diet. The top panel shows a number of fibers, while the lower panels show the boxed region at higher power. **K**. Histograms showing number of branches lost from NMJs of SD and HFD female at 9 months old. Scale bars: 10 μm and 50 μm (lowest magnification).

AChRs was significantly increased in HFD obese male mice compared to SD male mice. In female mice, however, there was no substantial loss of postsynaptic AChRs between the two viewings of the NMJs of HFD and SD mice (Figure 2C,F).

HFD-induced obese male mice had increased mortality (>50%) after surgical procedures and labeling receptors with bungarotoxin (probably because of anesthesia and labeling), so we performed additional experiments on fixed muscles. Sternomastoid muscles were fixed with PFA, bathed with BTX-Alexa488 (green) to label AChRs, which mark postsynaptic sites and fasciculin2-Alexa594 (red) to label acetylcholinesterase (AChEs, which mark the original location of the synapses) [31–33]. NMJs were then imaged with a high-resolution confocal microscope (Figure 2G,H) and the number of altered synapses with lost synaptic branches were quantified as the number of sites where a branch was visible on the red channel (AChEs) but not on the green channel (AChRs) (Figure 2I and Table 2). Of note, although AChE is a good marker for identifying traces of former synaptic sites that were lost (for several weeks), this approach will miss any branches for which both the AChR and AChE have disappeared, so the true number of lost synaptic branches in our snapshot images of NMJs may be underestimated. Nevertheless, using this approach, the general trend for a much higher loss of AChR expressing synaptic branches at synapses and an increase in number of altered NMJs of HFD than SD male mice was also found (Fig. 2I). In female mice, however, we didn't see any substantial damage of NMJs of HFD at ages of 6 and 9 months, comparable to NMJs of SD no-obese mice (Figure 2J,K). These observations suggest that sex differences strongly influence the effect of HFD-induced obesity on the damage of the neuromuscular system (see discussion).

Next, we examined whether obesity-related synaptic alterations in HFD obese male mice are associated with specific muscle fiber types and functions. For this, we used slow twitch soleus type I oxidative muscle and fast twitch extensor digitorum longus (EDL) type II glycolytic muscle of obese and age-matched SD mice. Because soleus and EDL are not amenable for multiple time lapse imaging, muscles were fixed and bathed with BTX-Alexa488 (green) and fasciculin2-Alexa594 (red). NMJs were imaged with the high-resolution confocal microscope and synaptic branches were quantified (Figure 3, Table 2). Table 2 shows that during early stages of obesity (4 months), few synaptic changes were observed and, as obesity was sustained, the severity of synaptic alterations increased (6 months and 9 months). In 9-month-old obese male mice, about half of NMJs had lost a significant number of synaptic branches and, in some cases, NMJs lost more than two-thirds of synaptic sites or entire synapses (sites that are easily recognizable by AChE staining but have no AChRs staining) (Figures 2 and 3). In age-matched non-obese mice, however, the majority of NMJs showed few synaptic alterations as evidenced by a perfect co-localization of AChE and AChR staining (Figures 2 and 3). These results suggest that obesity-related synaptic alterations are independent of muscle fiber types. Table 2 also shows that the number of eliminated synaptic branches is more prevalent in the sternomastoid than in leg muscles (EDL and soleus), suggesting that activity patterns of muscles may play an important role in regulating the postsynaptic disassembly.

The distribution pattern of AChRs at some NMJs of HFD obese mice was also abnormal. A close inspection of NMJs of non-obese mice revealed that AChRs normally have a smooth and continuous distribution and are confined within synaptic branches and perfectly co-localized with AChEs. In HFD obese mice, some areas of NMJs showed extended streaks and streams of AChRs beyond synaptic gutters (Fig. 3), suggesting a lateral diffusion of AChRs from their original synaptic sites into extra-synaptic areas. In most extreme cases, we observed the bulk of synaptic branches containing streaks of AChRs in the extrasynaptic areas. The abnormal AChR distribution pattern is more striking and frequent in soleus and, to some extent, in the EDL, but is rarely observed in the sternomastoid muscles. However, these abnormalities in the pattern of the AChR distribution were not observed in any of those muscles of age-matched non-obese male mice (Fig. 3).

The obesity-related synaptic alterations observed in male mice are different from those observed in muscle aging or muscle damage. In healthy aged mice (~24 months), NMJs are often fragmented into small islands, a hallmark of aged NMJs [34]. Most of the AChE staining sites also have AChRs staining, which differed significantly from alterations seen in NMJs of our adult obese mouse model (Figure 3 D). Also, the Haemotoxylin and Eosin staining of muscle sections from HFD obese male mice showed the absence of central nuclei (a marker of muscle degeneration and regeneration cycles) or fibrosis (Fig. 3E). No increase in creatine kinase activity [a marker of muscle damage; SD: 483 ± 126 U/L (n = 3 mice), HFD: 448 ± 154 U/L (n = 3 mice), p = 0.78] (Figure 4F) was detected in muscles of obese mice compared to mice fed with a standard diet. All together, these results strongly suggest that NMJs alterations seen in our obese mouse strain are not due to muscle degeneration/regeneration cycles.

3.3. Postsynaptic density, turnover rate of AChR, and presynaptic nerve terminals are impaired in obese mice

We asked whether the density of AChR in the remaining AChR-rich sites was altered in HFD obese mice. Sternomastoid muscles (at different stages of obesity) were saturated with a fluorescent BTX, imaged, and the fluorescence intensity of labled AChRs at NMJs was

Table 2 — Synaptic branch loss in fixed muscles.

Number of branch lost	sternomastoid						soleus						EDL					
	4 mo		6 mo		9 mo		4 mo		6 mo		9 mo		4 mo		6 mo		9 mo	
	SD	HFD**	SD	HFD†	SD	HFD†	SD	HFD [a]	SD	HFD**	SD	HFD†	SD	HFD [a]	SD	HFD*	SD	HFD†
0–1	132 (90%)	147 (72%)	96 (65%)	81 (47%)	72 (65%)	51 (32%)	38 (100%)	50 (96%)	40 (93%)	49 (68%)	159 (90%)	78 (56%)	40 (98%)	45 (92%)	28 (93%)	52 (76%)	105 (91%)	81 (58%)
2–5	14 (10%)	51 (25%)	51 (35%)	69 (40%)	35 (31%)	75 (46%)	0	2 (4%)	3 (7%)	23 (32%)	17 (10%)	54 (38%)	1 (2%)	4 (8%)	2 (7%)	16 (24%)	10 (9%)	52 (37%)
>6	0	7 (3%)	0	23 (13%)	4 (4%)	36 (22%)	0	0	0	0	0	8 (6%)	0	0	0	0	0	6 (4%)
Total NMJs	146	205	147	173	111	162	38	52	43	72	176	140	41	49	30	68	115	139

[a] Values are not statistically significant; *and ** values indicate significance compared to age-matched Standard Diet *(p<0.05 and p<0.001 respectively);*† Indicates significance compared to age-matched Standard Diet *(p<0.0001). 3–4 mice* per *diet* per *age.*

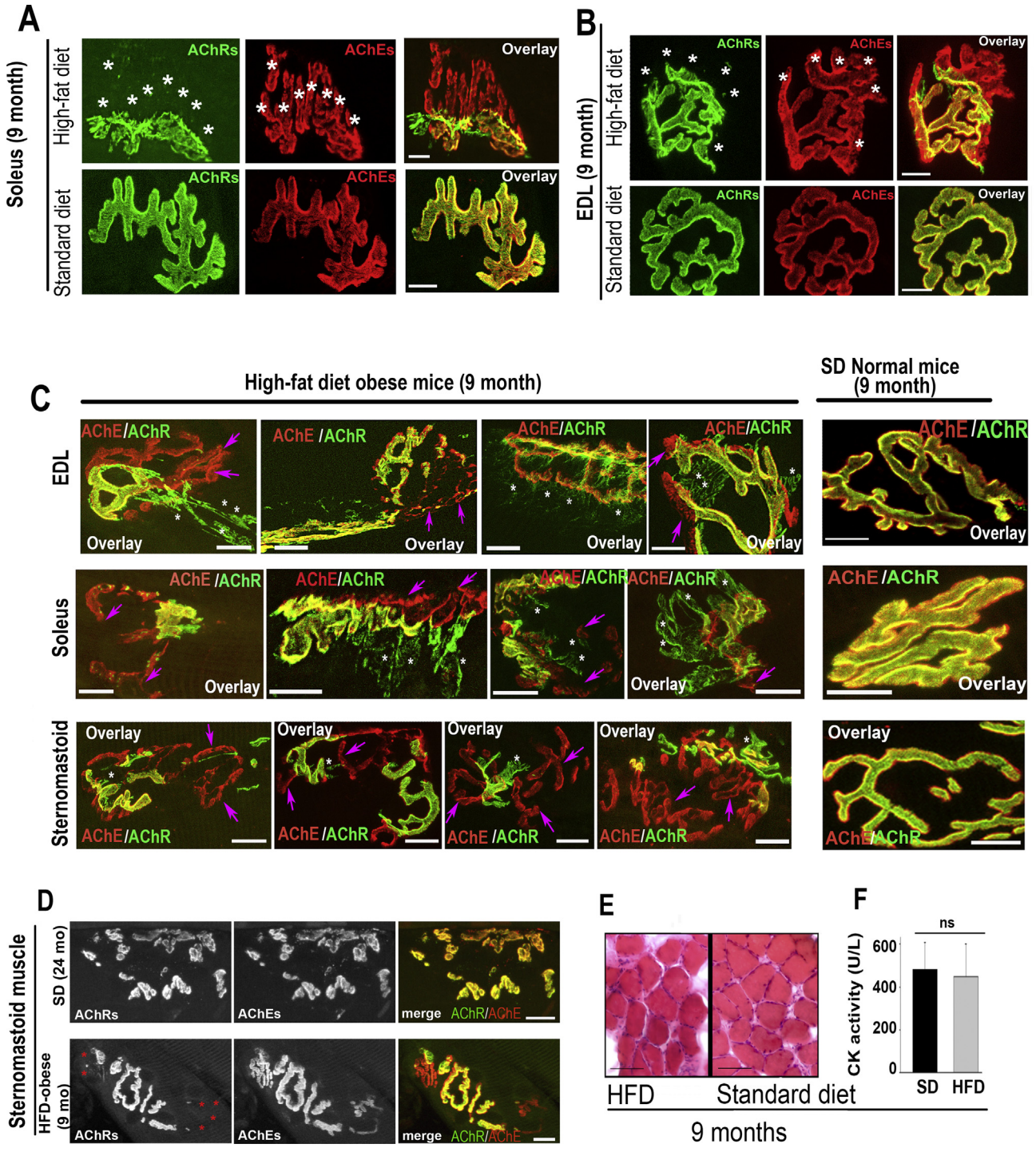

Figure 3: The disassembly of the postsynaptic apparatus and the abnormal AChR distribution pattern in HFD-induced obese mice is independent of muscle fiber types. A-B. Soleus and Extensor digitorum longus (EDL) muscles of 9-month-old obese (continuously fed with HFD) or non-obese male mice (fed with standard diet) were fixed, bathed with BTX-Alexa488 to label AChRs and fasciculin2-Alexa594 to label AChEs and then imaged with the confocal microscope. **A**. Example of soleus NMJs from HFD and SD mice. **B**. Example of EDL NMJs from HFD and SD mice. Scale bars: 10 μm. Note that both NMJs on both muscles display a significant loss of postsynaptic receptor regions identified by AChE staining (asterisks). **C**. Fast twitch extensor digitorum longus (EDL), slow twitch soleus, and sternomastoid muscles of 9-month-old HFD obese and age-matched non-obese male mice were fixed, bathed with BTX-Alexa488 (green) to label AChRs and fasciculin2-Alexa594 (red) to label AChEs. Shown are four examples of NMJs of each muscle displaying significant loss of postsynaptic receptor regions identified by AChE staining (pink color, arrows) and presence of steaks and streams of AChR (white color, asterisks) beyond synaptic gutters while AChRs at NMJs of non-obese mice are evenly distributed and confined within synaptic sites where they perfectly co-localized with AChEs. **D**. Examples of NMJs of a healthy aging muscle (24 months) showing AChR-rich islands co-localized with AChEs (top panels) and a 9-month-old HFD obese mouse showing loss of AChR clusters (asterisk, bottom panels). **E**. Sections of muscles from HFD obese and non-obese standard diet mice stained with hematoxylin and eosin showing an absence of central nuclei; **F**. Histogram showing no difference in creatine kinase activity (marker of muscle damage) in obese and non-obese muscles. Scale bars: 10 μm (A, B, C and D), 100 μm (E).

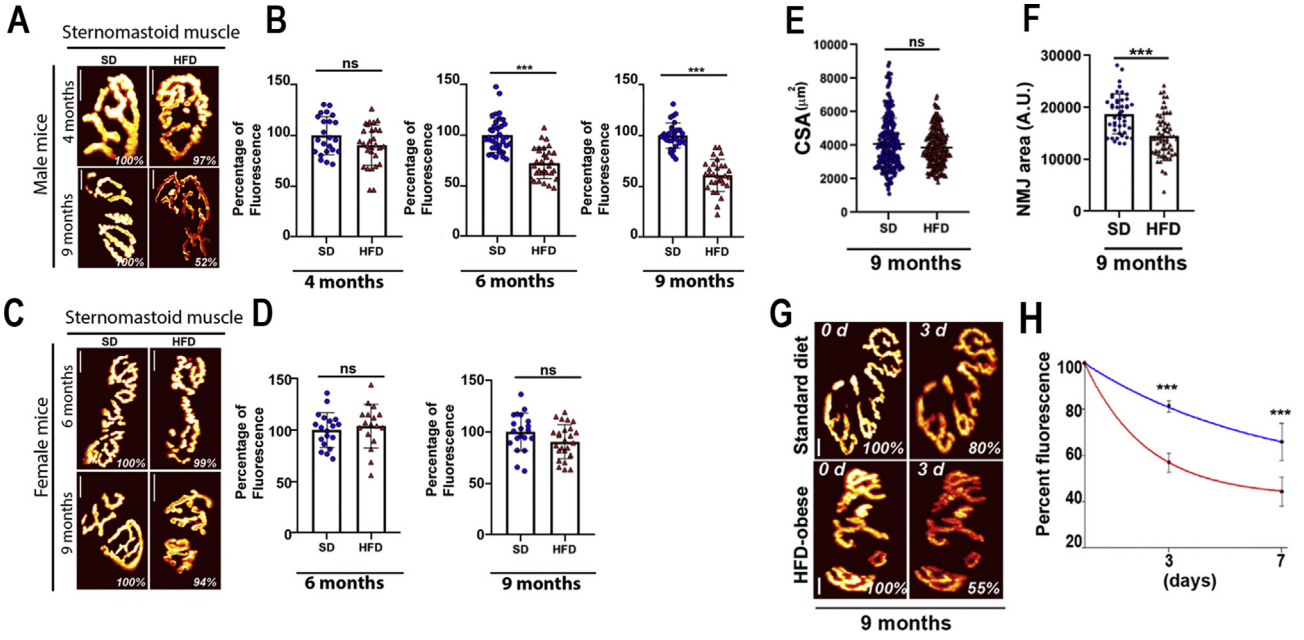

Figure 4: The density and the turnover rate of AChRs are significantly reduced in HFD obese male. The density of AChRs was assessed as described in Methods. **A**: Examples of NMJs of HFD male obese and non-obese SD mice (4 and 9 months) from sternomastoid muscles. **C**. Examples of NMJs of HFD female obese and non-obese SD mice (6 and 9 months) from sternomastoid muscles. The pseudo-color images provide a linear representation of the density of AChRs (white-yellow, high density; red-black, low density). **B.** Graphs summarizing the quantification of fluorescent data from male NMJs as shown in panel A at 4 months, 6 months (HFD: 72 ± 15% n = 31 NMJs from at least three animals; SD: 100 ± 16%, n = 37 NMJs at least from 3 animals; $p < 0.0001$), and 9 months old (HFD: 61 ± 15% n = 30 NMJs from at least three animals; standard diet: 100 ± 12%, n = 30 NMJs from at least 3 animals; $p < 0.0001$). **D.** Graphs summarizing the quantification of fluorescent data from female NMJs as shown in panel C at 6 months of age (HFD: 103 ± 16% n = 17 NMJs, three mice; standard diet: 100 ± 16%, n = 19 NMJs, three mice, $p = 0.56$) and 9 months of age (HFD: 91 ± 17% n = 26 NMJs, three mice; standard diet: 100 ± 18%, n = 20 NMJs, three mice, $p = 0.08$). Scale bars: 10 μm. **E**. Quantification of sternomastoid muscle fiber cross-sectional area from 9-month-old HFD obese and non-obese standard diet mice, (~250 fibers per diet). **F**. Quantification of synaptic area from 9-month HFD obese and non-obese standard diet mice (values are given as mean ± SD). **G**. Sternomastoid muscles of 9-month-old HFD obese and age-matched non-obese male mice were bathed with a low dose of fluorescent BTX and superficial NMJs were imaged and re-imaged 3 days later. The intensity of the fluorescence was measured at each time and the total fluorescence intensity of AChR was normalized to 100% at the initial imaging. Pseudo-color images provide a linear representation of the density of AChRs. **H**. Graph shows loss of fluorescently labeled AChRs from several synapses as illustrated in G. (Data are means ± SD). Scale bars: 10 μm.

then assayed. In obese male mice, during the early stage of obesity (up to 4 months), we did not observe any significant difference between the postsynaptic density of AChR of HFD obese and SD non-obese male mice in the three analyzed muscles. However, the density of AChR in sternomastoid muscle decreased by ~28% at 6 months of age and by 40% at 9 months (Figure 4A,B). A similar trend of reduced AChR density at the postsynaptic junction was also observed in soleus and EDL muscles (data not shown). Female mice, however, did not show any significant differences between the density of AChR in the sternomastoid muscle of HFD obese and SD non-obese mice at both 6 and 9 months of age (Figure 4C,D). Because there were no significant alterations at NMJs of female obese mice, we performed all remaining experiments on male mice.

We next measured muscle fiber cross sectional area (CSA) to determine whether muscle fiber size was affected by obesity. In the sternomastoid muscle of 9-month-old obese and non-obese male mice, we found that there was no significant difference in CSA between obese and non-obese mice (SD: 4075 ± 1550 μm^2 n = 5 mice; HFD: 3874 ± 1098 μm^2 n = 6 mice, $p = 0.11$. Values are given as mean ± SD) (Fig. 4E). Similar results were obtained in EDL and soleus (data not shown). However, measurements of the size of obese NMJs showed a significant reduction in NMJs compared to non-obese synapses (HFD: 14,442 ± 4178 A U. n = 65 NMJs; SD: 18,739 ± 3800 A U. n = 45 NMJs; $p < 0.0001$. Values are given as mean ± SD) (Fig. 4F). Taken together, these results indicate that the reduction of NMJs is not due to a decrease in muscle size, but rather to a disappearance of synaptic sites with AChRs.

Given the significant reduction in AChR density, we asked whether the turnover rate of AChRs was altered in HFD obese mice. The sternomastoid muscles of HFD obese and age-matched non-obese mice fed with SD were bathed with a non-saturating dose of BTX-Alexa488 (<30% of receptors were labeled, leaving synapses functional [21,25]), labeled AChRs were imaged, and the loss of fluorescently tagged AChRs was monitored over the next 7 days. At 7 days, we found that the remaining fluorescent intensity of the labeled receptors at NMJs of HFD obese mice was 45 ± 7%, n = 20 NMJs, 3 mice [$t_{1/2} \approx$ ~5.5 days] while in non-obese SD mice, the fluorescent intensity decreased more slowly (remaining fluorescence = 66 ± 8%, n = 27 NMJs, 4 mice [$t_{1/2} \approx$ ~11.3 days], $p < 0.0001$, (Data are means ± standard deviation) (Figure 4G—H). These results indicate that the half-life of AChRs at HFD obese synapses is ~2 times faster than AChR at NMJs of non-obese synapses.

As postsynaptic sites were eliminated in HFD-induced obese mice, it was possible that the overlying motor nerve terminals were also impaired. To test this, fixed sternomastoid muscles of HFD-induced obese and non-obese mice (7 to 9-month-old) were bathed with an antibody against neurofilament to label axons (green), and BTX-Alexa594 (labels AChRs). A close inspection of NMJs showed that in

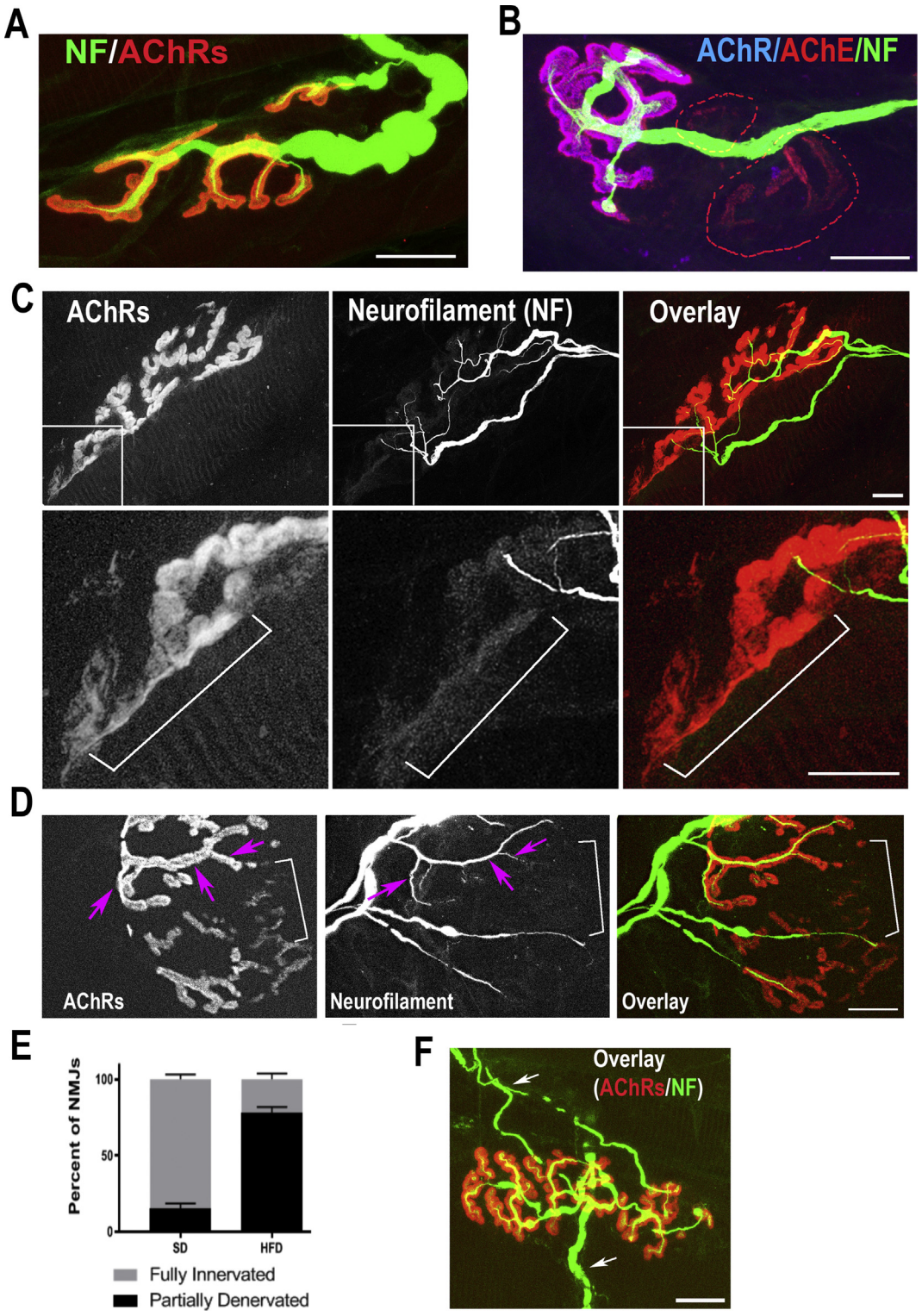

Figure 5: Presynaptic alterations in NMJs of male mice fed with HFD. The sternomastoid muscle of mice fed with high fat and standard diets were fixed and stained with BTX-Alexa549 to label AChR and with antibodies against neurofilament (green) to label axons. **A.** Example of an NMJ from an age-matched non-obese mouse fed the standard diet. **B.** Example of an NMJ from an HFD-obese mouse (7 months). The AChE (red) channel shows the original area of the synapse. The absence of overlying AChR (blue) and NF (green) signals from areas identified by AChEs staining (dashed lines) indicates regions where both axon terminals and AChRs were lost. **C.** A high-resolution confocal image of a representative NMJ from 9-month-old HFD-obese mouse displaying partial denervation. The inset images show faint AChR clusters (see bracket) without an overlying nerve terminal. **D.** Example of an NMJ of an HFD-obese mice (9 months) showing regions of high receptor density covered by the nerve terminal (arrows) and regions of low density of AChR devoid of nerves (brackets). **E.** Quantification of results from a series of synapses labelled with fluorescent BTX and neurofilament antibody. **F.** Example of an NMJ of an HFD-obese mouse (9 months) contacted by two axons (arrows). Scale bars: 10 μm.

non-obese mice (7- or 9-month-old) fed with SD, terminal axons looked healthy and most of AChR-rich postsynaptic sites were covered by axonal branches of a single motor axon (Figure 5A). However, in NMJs of age-matched HFD obese mice, branches of motor nerve terminals were no longer present in the areas where AChRs were missing (identified by AChE staining) (Fig. 5B). We also observed that many postsynaptic sites of HFD obese mice were partially occupied by axon branches, leaving other AChR sites denervated (Figure 5C,D). In some regions where nerve terminals were absent, AChRs were faintly stained (Figure 5C,D). Such abnormalities were not seen at NMJs of age-matched non-obese standard diet mice, in which all postsynaptic AChR-rich sites were occupied by nerve terminals (Fig. 5A). Quantification of the percentage of partially denervated NMJs where the presynaptic marker was missing from certain regions of AChR-rich postsynaptic sites showed that in non-obese 9-month-old mice fed with SD, the majority of synapses were fully innervated (84 $\pm$ 8%, n = 66 NMJs), while in obese HFD mice, only 22 $\pm$ 8.6%, (n = 68 NMJs) were fully innervated ($p < 0.0001$, Two-Way ANOVA) (Fig. 5E). We also observed in a few cases that NMJs of obese mice were dually innervated (Fig. 5F).

3.4. Obesity-related synaptic structural alterations after switching from HFD to a standard fat diet

We assessed whether obesity-related synaptic structural alterations were reversible. To accomplish this, following 6 months of HFD, obese mice were switched from an HFD to an SD for three months, and NMJ anatomical features (postsynaptic AChR density, number of synaptic sites lost, and the geometry of the postsynaptic apparatus) were analyzed. The body weight of obese mice was significantly reduced (from ~75 g to ~50 g) when HFD-obese mice were switched to an SD, comparable to the body weight of mice fed with an SD for the entire duration of the experiment (Figure 6A). Saturation of AChRs in the sternomastoid muscles of these mice with BTX-Alexa488 revealed that the density of AChR at NMJs was completely restored to normal AChR density (Figure 6B,C). Similar results were observed in the soleus and EDL, in which the density of AChR was also restored to normal non-obese mice (data not shown). However, the number of lost synaptic sites and the total areas of synapses identified by AChE staining remained significantly high compared to non-obese mice, comparable to NMJs size of HFD obese mice (Figure 6E,G), suggesting that the loss of synaptic sites is irreversible. Interestingly, the abnormalities in the AChR distribution pattern seen in some NMJs of HFD obese mice disappeared from non-synaptic regions when HFD obese mice were switched to SD (Fig. 6F).

4. DISCUSSION

In this work, we report substantial alterations in the neuromuscular system of male mice made obese by prolonged feeding with a high fat diet, while female mice were not significantly impaired (at least during the time window of our experiments). In contrast to normal healthy NMJs of age-matched mice fed with SD, we found that a significant number of NMJs of HFD-obese male mice displayed several abnormalities. First, the patterning of the postsynaptic AChRs became simplified, as many branches disappeared and the size of synapses was significantly reduced; in some cases, more than two-thirds of synaptic branches disappeared and, in a few cases, no AChR remained at the original synaptic site. Furthermore, streams and streaks of AChRs were observed in the extrasynaptic regions of some NMJs of HFD mice but not in SD mice. Second, the severity of the synaptic alterations became greater with long-term exposure to HFD. Third, the postsynaptic AChR density was significantly reduced and the turnover rate of AChR significantly increased in HFD obese mice. Fourth, nerve terminal branches were no longer present at many of the lost AChR rich regions. Fifth, the number of partially denervated muscle fibers was significantly increased. Sixth, when animals were switched from HFD to SD, both normal postsynaptic density and distribution patterns of AChR were restored, but a significant number of lost synaptic branches was not reversed. These results demonstrate that the neuromuscular system in HFD obese mice is susceptible to damage, which may impair synaptic strength and muscle function.

The model of HFD-induced obesity in male mice used in this study is an excellent tool to investigate the impact of obesity on the stability of the neuromuscular system. Mice are initially normal and become progressively heavier, mimicking human obesity. Importantly, mice did not develop type 2 diabetes or hyperglycemia (at least over the time window of our studies) (Fig. 1), so potential secondary consequences caused by diabetes will not interfere with the obesity effect. The morphological features of the altered NMJs in this obese mouse model did not resemble reported patterns of obesity-related NMJ alterations in diabetic mouse models, nor those in diabetic neuropathy in human or spontaneous diabetic rats [35,36], or abnormalities of synaptic fragmentation seen in aged skeletal muscle [34], or synaptic features in muscles undergoing degeneration/regeneration cycles [37,38]. While it is not clear whether compromised NMJs observed in our mouse model arise from obesity or/and HFD by itself, it is conceivable that the differences between altered NMJs in diabetic and non-diabetic obese mice may result from impairment of distinct signal transduction pathways.

The disassembly of the neuromuscular system in our HFD obese mice is a slow and gradual process. During the early stages of obesity (short-term HFD), only few synaptic branches were lost. However, in long-term HFD-induced obese mice, the disassembly of NMJs became more pronounced. It is not clear what stimulates the loss of some postsynaptic regions and why some synapses are more affected than others, but it is likely that obesity-induced disassembly of synapses is a multifactorial process. In long-term HFD-induced obese mice, it has been reported that enlarged adipose tissues substantially increased [39], leading to an increase in macrophage infiltration into adipose tissue [40] and a significant production of pro-inflammatory proteins [41]. In the central nervous system, it has been reported that structural and functional alterations of synapses in the hippocampus are associated with increased inflammation [42,43]. It is possible that similar mechanisms may occur in the neuromuscular system. Regardless of the mechanism, our results suggest that there must be a local change in normal regulatory mechanisms to cause a decrease in the density of molecules below a threshold value that initiates the irreversible removal of some synaptic clusters. Consistent with this, we have previously shown that a threshold density of AChRs likely provides a critical signal that enables the stability of postsynaptic proteins [44].

HFD had a significant impact on the disassembly of the neuromuscular system in obese male mice but not in obese female mice (at least during the time period of our studies). It is worth noting that male mice became obese at earlier time points of HFD feeding (after 2 months) than females (after 5–6 months of HFD feeding). Indeed, several studies have shown that female mice fed with HFD are resistant to developing weight gain and related metabolic changes [45–47], and they exhibit an increase in the anti-inflammatory cell population and a decrease in the population of pro-inflammatory macrophages [45,47]. Thus it is possible that in HFD female mice, sex hormones such as estrogen may protect obese female mice against induced HFD metabolic changes and the disassembly of synapses. Consistent with this, it

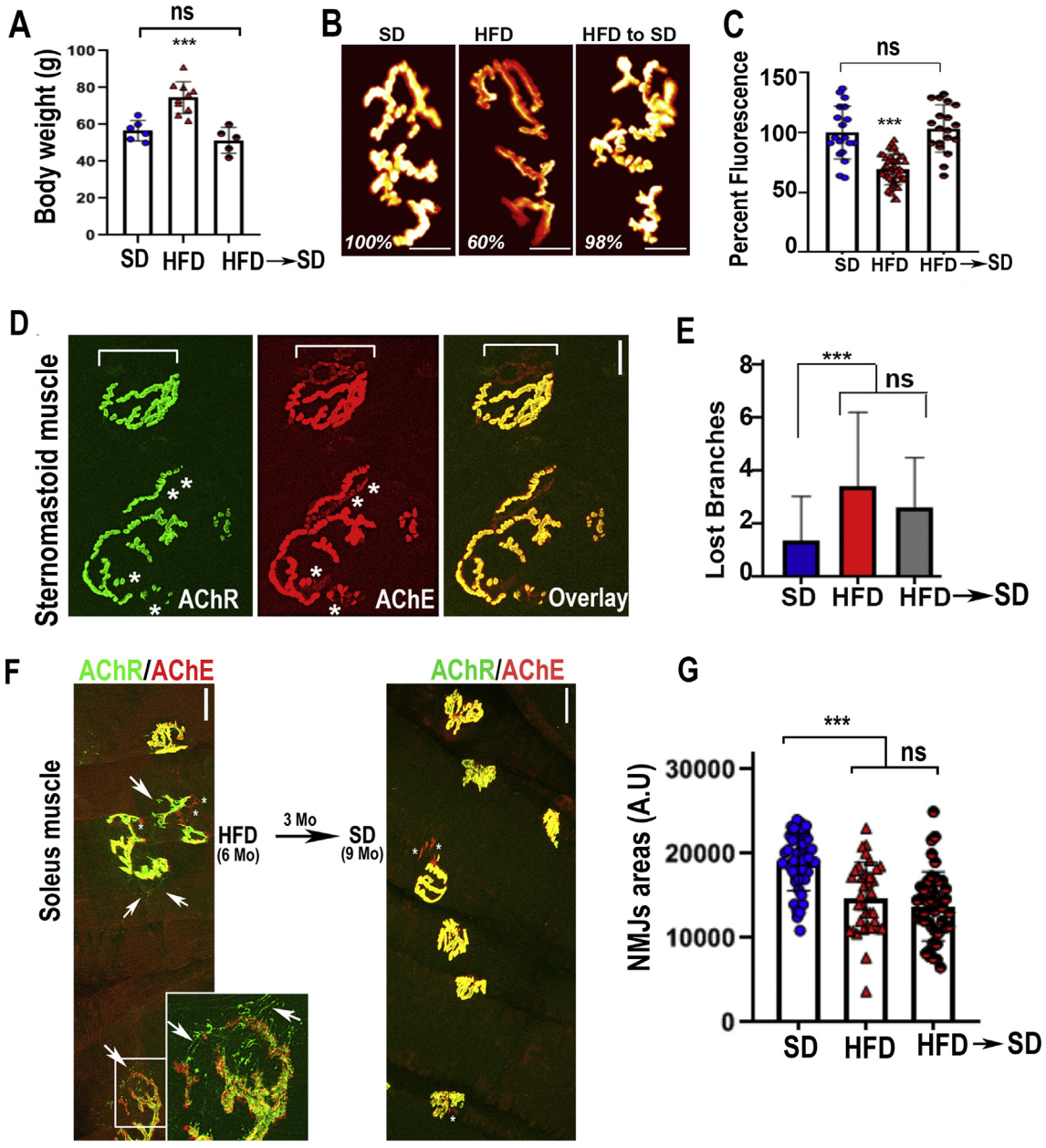

Figure 6: Structural alterations are irreversible after switching obese male mice from HFD to standard diet. Mice were fed for 6 months with the HFD and then switched to the SD for three months. **A.** Body weight of HFD obese mice after switching from HFD to SD compared to mice on the HFD or SD for the full 9 months. Note that the body weight of obese mice was significantly reduced (SD: 56.6 ± 5 g (six mice); HFD: 74.5 ± 8 g, (10 mice); HFD back to SD: 51.4 ± 7 g, (five mice). Data are means ± SD. **B**. Fluorescence intensity of labeled AChRs was measured and normalized to synapses kept on the SD for all 9 months. **C**, Summary of a series of experiments as in B. Note that the density of AChR at NMJs of HFD obese mice switched to standard diet was completely restored to normal AChR density (SD: 101 ± 20%, n = 19 NMJs, three mice; HFD: 66 ± 10% SD, n = 35 NMJs, four mice; and HFD switched to SD: 102 ± 19%, n = 19 NMJs, three mice, $p < 0.0001$, One-way ANOVA). Data are means ± SD. **D.** Confocal images of NMJs on sternomastoid muscle of HFD synapse switched to SD. **E.** Histogram showing number of lost synaptic branches from a series of experiments as in D (SD: 1.3 ± 0.16 (SEM), n = 111 NMJs, three mice; HFD: 3.4 ± 0.22 (SEM), n = 162 NMJs, four mice; and HFD switched to SD: 2.6 ± 0.24 (SEM), n = 59 NMJs, three mice, $p < 0.0001$, One-way ANOVA). **F.** Examples of NMJs from 6-month-old HFD obese mice displaying presence of AChRs in the extrasynaptic area (arrows) and loss of synaptic sites as marked by AChE staining (red color and white asterisks). The inset image shows streams and streaks of AChRs (green color) in the extrasynaptic regions (arrows). **G.** Quantification of NMJs areas from the three groups of mice (SD: 18,986 ± 3384, n = 41 NMJs, three mice; HFD: 14,780 ± 4165, n = 35 NMJs, four mice; and HFD switched to SD: 13,775 ± 4118, n = 43 NMJs, three mice, $p < 0.0001$, One-way ANOVA). Data are means ± SD. Scale bars for B and D: 10 μm, for F: 25 μm.

has been reported that HFD-impairments of learning functions and synaptic plasticity are more pronounced in HFD obese male mice than in female mice [48]. Accumulating evidence suggests that estrogen (as one of main female sex hormones), through binding to its receptors embedded in lipid rafts, promotes lipid raft homeostasis. Because lipid rafts are required for the clustering of AChRs in the postsynaptic membrane [49], it is plausible that sex hormones such as estrogen in female HFD obese mice may participate in the postsynaptic membrane

preservation, while in male mice, the high-fat diet may disrupt the lipid rafts domain, leading to postsynaptic receptor clusters disassembly. Further investigation is warranted to explore the effect of sex hormone depletion in HFD obese females, particularly during the post-menopausal periods.

An interesting finding of this work is the reversible changes in receptor density when HFD obese male mice lost body weight and became comparable to non-obese mice. The current results showed that the recovery of the density of AChR was only limited to the AChR remaining at postsynaptic sites; lost synaptic branches identified by AChE exhibited no recovery of AChRs. This is consistent with the idea that AChRs are required for the local maintenance and formation of new synaptic sites and once the receptors are eliminated, the entire modular units at AChR clusters are dissipated [44]. Changes in AChR density also occur during naturally occurring synapse elimination [29] and can be experimentally removed by locally altering postsynaptic activity at part of an NMJ before synapses withdraw [50]. It is possible that the phenomenon of the postsynaptic disassembly observed in HFD obese mice may use the same mechanism involved in synapse elimination during normal and pathological conditions. While it is unclear how obesity regulates the density of AChRs, it is strongly suggestive that the degeneration of the postsynaptic density/apparatus is correlated with the accumulation of adipose tissues.

FUNDING

This work was supported by the National Institute for Neurological Disorders and Stroke (*NINDS*), USA (Grants NS-047332 and NS-103845 to Akaaboune), and the University of Michigan.

AUTHOR CONTRIBUTIONS

Conceptualization: M.A. and I.M.V. Methodology: M.A and I.M.V. Writing and editing: M.A and I.M.V. Supervision: M.A

ACKNOWLEDGEMENT

We thank Drs. Richard Hume and Laura Smithson (University of Michigan) for critical comments on this manuscript and Akaaboune laboratory members for technical assistance and comments on this manuscript.

CONFLICT OF INTERESTS

The authors declare that they have no known competing financial interests or personal relationships that could have appeared to influence the work reported in this paper.

REFERENCES

[1] Pi-Sunyer, X., 2009. The medical risks of obesity. Postgraduate Medical Journal 121(6):21—33.

[2] Nuttall, F.Q., 2015. Body mass index: obesity, BMI, and Health: a critical review. Nutrition Today 50(3):117—128.

[3] Goodpaster, B.H., Krishnaswami, S., Harris, T.B., Katsiaras, A., Kritchevsky, S.B., Simonsick, E.M., et al., 2005. Obesity, regional body fat distribution, and the metabolic syndrome in older men and women. Archives of Internal Medicine 165(7):777—783.

[4] Zhang, Y., Proenca, R., Maffei, M., Barone, M., Leopold, L., Friedman, J.M., 1994. Positional cloning of the mouse obese gene and its human homologue. Nature 372(6505):425—432.

[5] Chen, H., Charlat, O., Tartaglia, L.A., Woolf, E.A., Weng, X., Ellis, S.J., et al., 1996. Evidence that the diabetes gene encodes the leptin receptor: identification of a mutation in the leptin receptor gene in db/db mice. Cell 84(3):491—495.

[6] Lee, G.H., Proenca, R., Montez, J.M., Carroll, K.M., Darvishzadeh, J.G., Lee, J.I., et al., 1996. Abnormal splicing of the leptin receptor in diabetic mice. Nature 379(6566):632—635.

[7] Huszar, D., Lynch, C.A., Fairchild-Huntress, V., Dunmore, J.H., Fang, Q., Berkemeier, L.R., et al., 1997. Targeted disruption of the melanocortin-4 receptor results in obesity in mice. Cell 88(1):131—141.

[8] Chen, A.S., Metzger, J.M., Trumbauer, M.E., Guan, X.M., Yu, H., Frazier, E.G., et al., 2000. Role of the melanocortin-4 receptor in metabolic rate and food intake in mice. Transgenic Research 9(2):145—154.

[9] Chua, S.C., Chung, W.K., WuPeng, X.S., Zhang, Y.Y., Liu, S.M., Tartaglia, L., et al., 1996. Phenotypes of mouse diabetes and rat fatty due to mutations in the OB (leptin) receptor. Science 271(5251):994—996.

[10] Wang, C.Y., Liao, J.K., 2012. A mouse model of diet-induced obesity and insulin resistance. Methods in Molecular Biology 821:421—433.

[11] Rossmeisl, M., Rim, J.S., Koza, R.A., Kozak, L.P., 2003. Variation in type 2 diabetes–related traits in mouse strains susceptible to diet-induced obesity. Diabetes 52(8):1958—1966.

[12] Speakman, J., Hambly, C., Mitchell, S., Krol, E., 2007. Animal models of obesity. Obesity Reviews 8(Suppl 1):55—61.

[13] Wahba, I.M., Mak, R.H., 2007. Obesity and obesity-initiated metabolic syndrome: mechanistic links to chronic kidney disease. Clinical Journal of the American Society of Nephrology 2(3):550—562.

[14] Jurdak, N., Lichtenstein, A.H., Kanarek, R.B., 2008. Diet-induced obesity and spatial cognition in young male rats. Nutritional Neuroscience 11(2):48—54.

[15] Murray, A.J., Knight, N.S., Cochlin, L.E., McAleese, S., Deacon, R.M., Rawlins, J.N., et al., 2009. Deterioration of physical performance and cognitive function in rats with short-term high-fat feeding. The FASEB Journal 23(12):4353—4360.

[16] Bocarsly, M.E., Fasolino, M., Kane, G.A., LaMarca, E.A., Kirschen, G.W., Karatsoreos, I.N., et al., 2015. Obesity diminishes synaptic markers, alters microglial morphology, and impairs cognitive function. Proceedings of the National Academy of Sciences of the United States of America 112(51):15731—15736.

[17] Molteni, R., Barnard, R.J., Ying, Z., Roberts, C.K., Gomez-Pinilla, F., 2002. A high-fat, refined sugar diet reduces hippocampal brain-derived neurotrophic factor, neuronal plasticity, and learning. Neuroscience 112(4):803—814.

[18] Cristino, L., Busetto, G., Imperatore, R., Ferrandino, I., Palomba, L., Silvestri, C., et al., 2013. Obesity-driven synaptic remodeling affects endocannabinoid control of orexinergic neurons. Proceedings of the National Academy of Sciences of the U S A 110(24):E2229—E2238.

[19] Massa, F., Mancini, G., Schmidt, H., Steindel, F., Mackie, K., Angioni, C., et al., 2010. Alterations in the hippocampal endocannabinoid system in diet-induced obese mice. Journal of Neuroscience 30(18):6273—6281.

[20] Jagust, W., Harvey, D., Mungas, D., Haan, M., 2005. Central obesity and the aging brain. Archives of Neurology 62(10):1545—1548.

[21] Akaaboune, M., Culican, S.M., Turney, S.G., Lichtman, J.W., 1999. Rapid and reversible effects of activity on acetylcholine receptor density at the neuromuscular junction in vivo. Science 286(5439):503—507.

[22] >Martinez-Pena y Valenzuela, I., Mouslim, C., Pires-Oliveira, M., Adams, M.E., Froehner, S.C., Akaaboune, M., 2011. Nicotinic acetylcholine receptor stability at the NMJ deficient in alpha-syntrophin in vivo. Journal of Neuroscience 31(43):15586—15596.

[23] Turney, S.G., Culican, S.M., Lichtman, J.W., 1996. A quantitative fluorescence-imaging technique for studying acetylcholine receptor turnover at neuromuscular junctions in living animals. Journal of Neuroscience Methods 64(2):199—208.

[24] Valenzuela, I.M.P.Y., Pires-Oliveira, M., Akaaboune, M., 2013. PKC and PKA regulate AChR dynamics at the neuromuscular junction of living mice. PloS One 8(11).

[25] Martinez-Pena, Y.V.I., Aittaleb, M., Chen, P.J., Akaaboune, M., 2015. The knockdown of alphakap alters the postsynaptic apparatus of neuromuscular junctions in living mice. Journal of Neuroscience 35(13):5118—5127.

[26] Darimont, C., Delansorne, R., Paris, J., Ailhaud, G., Negrel, R., 1997. Influence of estrogenic status on the lipolytic activity of parametrial adipose tissue in vivo: an in situ microdialysis study. Endocrinology 138(3):1092—1096.

[27] Cao, J.J., Gregoire, B.R., 2016. A high-fat diet increases body weight and circulating estradiol concentrations but does not improve bone structural properties in ovariectomized mice. Nutrition Research 36(4):320—327.

[28] Rich, M.M., Lichtman, J.W., 1989. In vivo visualization of pre- and post-synaptic changes during synapse elimination in reinnervated mouse muscle. Journal of Neuroscience 9(5):1781—1805.

[29] Balice-Gordon, R.J., Lichtman, J.W., 1993. In vivo observations of pre- and postsynaptic changes during the transition from multiple to single innervation at developing neuromuscular junctions. Journal of Neuroscience 13(2):834—855.

[30] Wigston, D.J., 1989. Remodeling of neuromuscular junctions in adult mouse soleus. Journal of Neuroscience 9(2):639—647.

[31] Schmidt, N., Akaaboune, M., Gajendran, N., Martinez-Pena y Valenzuela, I., Wakefield, S., Thurnheer, R., et al., 2011. Neuregulin/ErbB regulate neuromuscular junction development by phosphorylation of alpha-dystrobrevin. The Journal of Cell Biology 195(7):1171—1184.

[32] Peng, H.B., Xie, H.B., Rossi, S.G., Rotundo, R.L., 1999. Acetylcholinesterase clustering at the neuromuscular junction involves perlecan and dystroglycan. Journal of Cell Biology 145(4):911—921.

[33] Scott, L.J.C., Bacou, F., Sanes, J.R., 1988. A synapse-specific carbohydrate at the neuromuscular-junction - association with both acetylcholinesterase and a glycolipid. Journal of Neuroscience 8(3):932—944.

[34] Valdez, G., Tapia, J.C., Kang, H., Clemenson, G.D., Gage, F.H., Lichtman, J.W., et al., 2010. Attenuation of age-related changes in mouse neuromuscular synapses by caloric restriction and exercise. Proceedings of the National Academy of Sciences of the United States of America 107(33): 14863—14868.

[35] Fahim, M.A., Hasan, M.Y., Alshuaib, W.B., 2000. Early morphological remodeling of neuromuscular junction in a murine model of diabetes. Journal of Applied Physiology 89(6):2235—2240.

[36] Mendell, J.R., Sahenk, Z., Warmolts, J.R., Marshall, J.K., Thibert, P., 1981. The spontaneously diabetic bb wistar rat - morphologic and Physiologic studies of peripheral-nerve. Journal of the Neurological Sciences 52(1):103—115.

[37] Grady, R.M., Teng, H., Nichol, M.C., Cunningham, J.C., Wilkinson, R.S., Sanes, J.R., 1997. Skeletal and cardiac myopathies in mice lacking utrophin and dystrophin: a model for Duchenne muscular dystrophy. Cell 90(4):729—738.

[38] Akaaboune, M., Grady, R.M., Turney, S., Sanes, J.R., Lichtman, J.W., 2002. Neurotransmitter receptor dynamics studied in vivo by reversible photounbinding of fluorescent ligands. Neuron 34(6):865—876.

[39] Jung, U.J., Choi, M.S., 2014. Obesity and its metabolic complications: the role of adipokines and the relationship between obesity, inflammation, insulin resistance, dyslipidemia and nonalcoholic fatty liver disease. International Journal of Molecular Sciences 15(4):6184—6223.

[40] Weisberg, S.P., McCann, D., Desai, M., Rosenbaum, M., Leibel, R.L., Ferrante, A.W., 2003. Obesity is associated with macrophage accumulation in adipose tissue. Journal of Clinical Investigation 112(12):1796—1808.

[41] Fried, S.K., Bunkin, D.A., Greenberg, A.S., 1998. Omental and subcutaneous adipose tissues of obese subjects release interleukin-6: depot difference and regulation by glucocorticoid. Journal of Clinical Endocrinology & Metabolism 83(3):847—850.

[42] Dinel, A.L., Andre, C., Aubert, A., Ferreira, G., Laye, S., Castanon, N., 2011. Cognitive and emotional alterations are related to hippocampal inflammation in a mouse model of metabolic syndrome. PloS One 6(9):e24325.

[43] Grillo, C.A., Piroli, G.G., Junor, L., Wilson, S.P., Mott, D.D., Wilson, M.A., et al., 2011. Obesity/hyperleptinemic phenotype impairs structural and functional plasticity in the rat hippocampus. Physiology & Behavior 105(1):138—144.

[44] Bruneau, E.G., Brenner, D.S., Kuwada, J.Y., Akaabounel, M., 2008. Acetylcholine receptor clustering is required for the accumulation and maintenance of scaffolding proteins. Current Biology 18(2):109—115.

[45] Pettersson, U.S., Walden, T.B., Carlsson, P.O., Jansson, L., Phillipson, M., 2012. Female mice are protected against high-fat diet induced metabolic syndrome and increase the regulatory T cell population in adipose tissue. PloS One 7(9).

[46] Bruder-Nascimento, T., Ekeledo, O.J., Anderson, R., Le, H.B., de Chantemele, E.J.B., 2017. Long term high fat diet treatment: an appropriate approach to study the sex-specificity of the autonomic and cardiovascular responses to obesity in mice. Frontiers in Physiology 8.

[47] Singer, K., Maley, N., Mergian, T., DelProposto, J., Cho, K.W., Zamarron, B.F., et al., 2015. Differences in hematopoietic stem cells contribute to sexually dimorphic inflammatory responses to high fat diet-induced obesity. Journal of Biological Chemistry 290(21):13250—13262.

[48] Hwang, L.L., Wang, C.H., Li, T.L., Chang, S.D., Lin, L.C., Chen, C.P., et al., 2010. Sex differences in high-fat diet-induced obesity, metabolic alterations and learning, and synaptic plasticity deficits in mice. Obesity 18(3):463—469.

[49] Zhu, D., Xiong, W.C., Mei, L., 2006. Lipid rafts serve as a signaling platform for nicotinic acetylcholine receptor clustering. Journal of Neuroscience 26(18): 4841—4851.

[50] Balice-Gordon, R.J., Lichtman, J.W., 1994. Long-term synapse loss induced by focal blockade of postsynaptic receptors. Nature 372(6506):519—524.

